8-25-2009

Mapping Donor Electrn Wave Function Deformations at Sub-Bohr Orbit Resolution

Seung H. Park
Purdue University - Main Campus

Rajib Rahman
Purdue University - Main Campus

Gerhard Klimeck
Purdue University - Main Campus, gekco@purdue.edu

Lloyd C. L. Hollenberg
University of Melbourne

Mapping donor electron wave function deformations at sub-Bohr orbit resolution

Seung H. Park,[1] Rajib Rahman,[1] Gerhard Klimeck,[1,2] and Lloyd C. L. Hollenberg[3]

[1]*Network for Computational Nanotechnology, Purdue University, West Lafayette, IN 47907, USA*
[2]*Jet Propulsion Laboratory, California Institute of Technology, Pasadena, CA 91109, USA*
[3]*Center for Quantum Computer Technology, School of Physics, University of Melbourne, VIC 3010, Australia*

(Dated: August 25, 2009)

Quantum wave function engineering of dopant-based Si nano-structures reveals new physics in the solid-state, and is expected to play a vital role in future nanoelectronics. Central to any fundamental understanding or application is the ability to accurately characterize the deformation of the electron wave functions in these atom-based structures through electromagnetic field control. We present a method for mapping the subtle changes that occur in the electron wave function through the measurement of the hyperfine tensor probed by ^{29}Si impurities. Our results show that detecting the donor electron wave function deformation is possible with resolution at the sub-Bohr radius level.

PACS numbers: 71.55.Cn, 03.67.Lx, 71.70.Ej, 85.35.Gv

The exponential miniaturization of semiconductor technology over the past 50 years has ushered in an era of nano-scale quantum electronics. At near atomic dimensions, conventional device operations are strongly affected by quantum phenomena in the solid-state [1, 2]. To ensure continued progress in semiconductor electronics, and indeed in the drive for new quantum nano-electronic devices, the inherently quantum aspects of such systems need to be understood and even incorporated into device functionality. The possibility of harnessing quantum phenomena in devices has produced revolutionary ways of performing computing, as exemplified by the rapidly developing fields of quantum computing and spintronics [3]. A central concept of quantum nano-electronics is the ability to induce controlled deformation of a specific donor-bound electron wave function by external electro-magnetic fields. Accessing the details of such wave function engineering is critical to understanding and developing new devices and applications. However, until now there has been no way of quantifying the type and nature of such wave function distortions beyond indirect means [1].

In this paper, we propose an electron-nuclear double resonance (ENDOR) experiment to directly measure the gate induced Stark shift of the donor electron hyperfine tensor at specific lattice sites near the donor site (Figure 1). Individual ^{29}Si atoms at random in the lattice provide a direct nuclear spin probe of the donor electron wave function within the Bohr orbit region. Our large scale atomistic tight-binding simulations for large lattice regions involving over a million atoms, show that this technique provides a spatial map of the bound donor electron response to a controlling gate field to sub-Bohr orbit resolution, with excellent correlation to the deformed electronic wave function, and confirm the feasibility of detecting such field induced hyperfine resonance shifts. The technique has wide applicability as it can in principle be extended to map out electric field response of wave functions in single electron Si quantum dots, quantum wells or other nano-structures. The ability to map single electron wave function distortions in this fashion may have far reaching consequences for many current and future quantum nano-electronic applications.

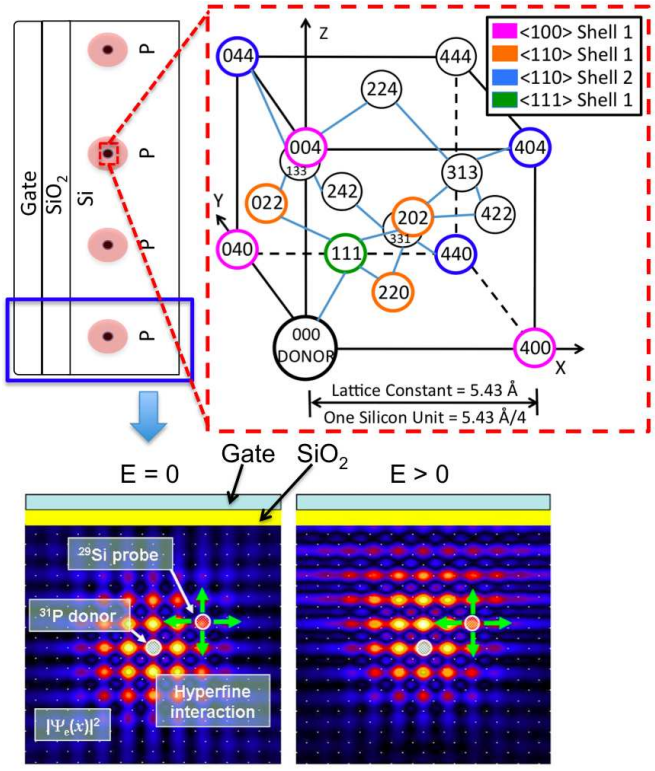

FIG. 1: Schematic of the technique. Top row: A series of donors in Si under a gate. Inset shows classification of the sub-Bohr radii region into symmetry classes and shells. Bottom row: Probing the field-induced distortions of the donor wavefunction by a ^{29}Si atom using hyperfine interaction.

Silicon-based quantum nano-electronic systems posses inherent advantages of long spin coherence times and vast expertise of the semiconductor industry in scalable system design and manufacture. As a result there are

a number of key proposals for quantum computing devices, including substitutional donors [4, 5, 6, 7, 8, 9], gate-confined 2DEGs [10], and Si quantum wells [11]. Advances in single atom [12] and ion implantation [13] technologies have opened the possibility of fabricating dopant based nano-structures in the laboratory in a repeatable manner. Some of the recent structures include a single gated donor in a FINFET [1, 2], a gated two donor charge qubit [14], a 2D gated donor layer [15], and an 1D metallic wire of donors between contacts [16]. The wave functions of such donor based nano-structures vary considerably from their bulk counterparts, yet are critical to device operation. A direct map of the wave functions and their electric field response will be of enormous importance in novel quantum device design and engineering.

The method we described here uses the hyperfine interaction between a donor bound electron spin and a nuclear spin of a ^{29}Si isotope in a lattice of spinless ^{28}Si atoms, similar to the method used by Hale and Mieher [17], but critically we include and analyse the effect of a controlling field deforming the donor wave function. The isotropic interaction (Fermi contact) can provide a direct measure of the electron probability density at a ^{29}Si lattice site, while the dipolar or anisotropic part yields information on the wave function around the ^{29}Si site. Although current technology limits the replacement of a ^{28}Si atom by a ^{29}Si atom at a specific point in the lattice, it is nevertheless possible to prepare device samples with an ensemble of ^{29}Si atoms distributed randomly around a gated donor simply for experimental characterization. The resonance peaks in the ENDOR frequencies[17] represent spin transitions of the donor-nucleus system and varies with distance from the donor.

ENDOR measurements were performed, first by Feher [18], and later by Hale and Mieher [17] to study parts of the ground state wave function of a donor close to the nucleus. The hyperfine tensors of almost 20 shells (Fig 1) were resolved for three donor species in Ref [17]. Hale and Mieher [19] used effective mass theory (EMT) and a method of equivalent orbitals to calculate hyperfine tensor of a few shells with semi-quantitative agreement with their experiment. Later, Ivey and Mieher [20] used a comprehensive numerical approach with a basis of pseudo-potential Bloch wavefunctions to improve the theoretical results. A recent ab-initio DFT study was able to calculate very accurately the tensor components of a few shells in the vicinity of the donor nucleus [21]. Hale and Castner [22] had measured changes in Fermi contact hyperfine constants under a uni-directionally applied stress. It was also shown [23] that inclusion of the anisotropic hyperfine in spin coherence time calculations provides remarkable agreement between theory and recent measurements. The only work on the Stark shift of the hyperfine tensors to date was done by Debernardi [24], who computed the Fermi contact coupling for 3 sites of a shell near the donor.

The hyperfine interaction between a donor electron spin S and an ^{29}Si nuclear spin I is $H = \vec{I} \cdot A \cdot \vec{S}$. Taking the origin at the ^{29}Si nucleus, the hyperfine tensor is,

$$A_{ij} = \gamma_I \gamma_S \hbar^2 \left(\frac{8\pi}{3} |\Psi(0)|^2 + \langle \Psi | \frac{3 r_i r_j - r^2 \delta_{ij}}{r^5} | \Psi \rangle \right) \quad (1)$$

where γ_I and γ_S are the nuclear and electronic gyromagnetic ratio respectively, and $r_{i,j} = (x, y, z)$. The first term in (1) is the Fermi contact hyperfine interaction, denoted here as β, and is directly proportional to the electronic probability density at the ^{29}Si site. The second term represents the magnetic dipolar or anisotropic hyperfine interaction between the two spins, and is often denoted as B_{ij}. A symmetrically distributed wave function about the probe nucleus will yield a negligible value for the anisotropic part, and the contact term dominates. Since in general the donor wave function is not symmetric about a given ^{29}Si site, the dipolar term contributes to the ENDOR resonance energies providing information about the overall distribution from that probe site.

The single donor wave functions subjected to constant electric fields were computed using an atomistic semi-empirical tight-binding (TB) model involving a 20 orbital per atom basis of sp^3d^5s* (spin) orbitals with nearest neigbour interactions. The TB model parameters were fine tuned by a genetic algorithm to fit the bulk Si bandstructure [25], and the donor was represented by a Coulomb potential with a cut-off term U_0 at the donor site adjusted to reproduce the experimental Si:P spectrum [26]. The total Hamiltonian including the externally applied field was diagonalized by a parallel Lanczos eigensolver to obtain the low lying donor electron states. These wave functions were used to evaluate the hyperfine tensors from equation (1) for all possible positions of the ^{29}Si probe in the lattice. The tight-binding method used here is embeded in the Nano-Electronic Modeling Tool (NEMO-3D) [27, 28], and had been successfully applied to compute Stark shift of the hyperfine coupling between a donor and its nucleus [29] in good agreement with experiments [30] and with momentum space methods [31]. The method was also used to investigate the orbital Stark shift of a donor-interface well system, and was verified with single donor transport experiments in FINFETs [1].

One of the most challenging aspects of this experiment is to identify which ^{29}Si site is responsible for a particular hyperfine peak. In order to simplify data analysis, the ^{29}Si lattice sites can be conveniently classified into shells and symmetry classes. For an unperturbed lattice, a shell is the group of equivalent lattice sites equidistant from the donor. Given the hyperfine tensors of one site in the shell, it is possible to obtain the tensors of all the other points by symmetry. The shells relevant in this work can be grouped into 3 symmetry classes. The $\langle 001 \rangle$ axis class contains all points an integral number of unit cells away

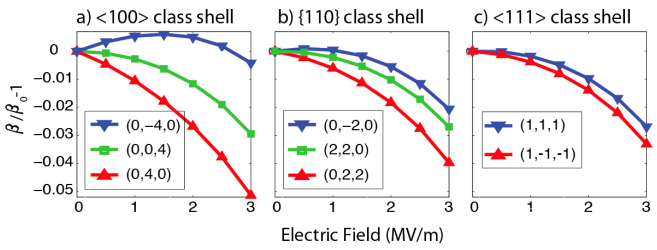

FIG. 2: Normalized relative change in the contact hyperfine coupling β as a function of electric field for the nearest shells of Classes a) $\langle 100\rangle$ b) $\{110\}$ c) $\langle 111\rangle$. The points in the shell are subdivided into sets, each having a different evolution pattern with the field.

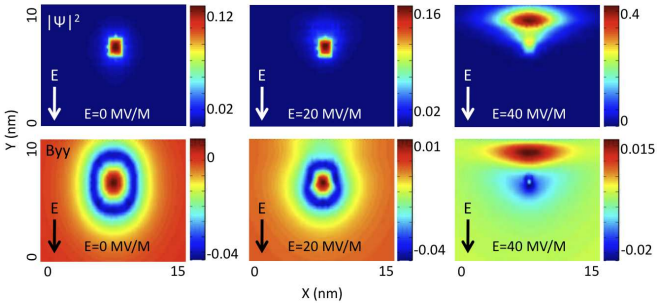

FIG. 3: Top panel: The P donor GS wavefunction at three different electric fields. Bottom Panel: the corresponding hyperfine maps in the form of B_{yy} tensor component. The E-field is in-plane with the xy-plane cut shown here.

from the donor. A particular shell of this class has 6 lattice sites with two of the coordinates zero. The $\{110\}$ plane class comprises all sites with two of the coordinates equal in magnitude and non-zero, and has 12 members per shell. The $\langle 111\rangle$ axis class contains all points with three coordinates equal in magnitude and non-zero, and has 4 members per shell. For example, the 4 nearest neighbors of the impurity form the 1st shell of the $\langle 111\rangle$ axis class. In this work, we concern ourselves with lattice sites within the Bohr radii only as this is the region of interest.

Without any external perturbations, all the points in a shell contribute to the same hyperfine peak. In the presence of an electric field, some members of a shell are no longer equivalent, and the hyperfine peak may split into several components. The non-equivalent members of a shell can further be classified into sets of points. In this work, we applied a constant electric field directed along the [010] direction of the crystal, and analyzed its effect on two shells of each of the 3 classes. Under such an electric field, a shell belonging to the $\langle 001\rangle$ axis class subdivides into 3 sets of points. Out of the 6 points, the 4 points with $y = 0$ are invariant with respect to the y-directed field and form a set. On the other hand, the points $(0, m, 0)$ and $(0, \bar{m}, 0)$ lie along the field and are each at different potential, each forming a different set. Each set within a shell is characterized by a distinct field response. This is evident in Fig 2a which plots the relative change in the contact hyperfine coupling β with electric field for the 1st shell of $\langle 001\rangle$ class. The 12 lattice sites associated with an $\{110\}$ shell can have 3 distinct y-coordinates, and will form 3 different sets, as corroborated by the 3 curves of Fig 2b. Similarly, an $\langle 111\rangle$ shell having 4 sites forms 2 sets as the electric field separates them in potential, as shown in Fig 2c. For more distant shells of the same class, the gap between the curves will increase as more potential drops between the sets.

The hyperfine tensors of the donor wave function experience both quadratic and linear Stark shifts, which can be described by the equation,

$$\Delta\alpha(\vec{E}) = \alpha(0)(\eta_2 E^2 + \eta_1 E) \qquad (2)$$

where $\alpha = (\beta, B_{ij})$, η_2 and η_1 are the quadratic and the linear Stark coefficients respectively. The curves obtained from our calculations for all the non-equivalent sets of a shell are fit to (2), and η_2 and η_1 are extracted and listed in Table 1. The usefulness of this table is underscored by the fact that given the tensor components at $E = 0$ for a shell and an applied field value, one can calculate both the Fermi contact hyperfine coupling and the dipolar tensor components, and obtain the actual hyperfine resonance frequency at that given field.

Fig. 3 shows the wavefunction of a P donor at 3.8 nm depth from the oxide interface subjected to electric fields 0, 20 and 40 MV/m. In this regime, the donor wavefunction can be modified adiabatically by the field [9, 31, 32, 33], as the electron makes a transition from a purely Coulomb confined state at $E = 0$ to a purely 2D confined state at the interface at $E = 40$ MV/m. In the intermediate field ($E = 20$ MV/m) regime, the electron resides in a superposition of Coulomb bound and surface bound states, as seen in the middle column of Fig 3. This serves an example of controlled wavefunction engineering by electric fields. An associated dipolar tensor component, B_{yy} for example, is shown on the 2nd row of Fig 3, and reflects the gradual symmetry change of the donor wavefunction.

To determine whether it is feasible to measure the Stark shift of a nearby shell, we perform an example calculation for the 1st shell of $\langle 001\rangle$ class. Table II of Ref [17] reported the zero-field hyperfine frequencies of β and B_{zz} for this shell to be 2981 and 41.4 kHz respectively. With $E = 4$ MV/m, and using Table I and equation (2) of this paper, we predict that a and B_{zz} of the site $(0, 4, 0)$ decrease by 243 and 3.3 kHz respectively, a net change which should be experimentally detectable. In comparison, the other two sets, $(0, \bar{4}, 0)$ and $(0, 0, 4)$, are shifted by 55 and 160 kHz in a and 0.7 and 2.2 kHz in B_{zz} respectively. Therefore, the 3 sets of this shell should be experimentally distinguishable under an applied field, in this case primarily due to the Fermi contact coupling.

In conclusion, we propose the measurement of hyper-

TABLE I: Qudratic (η_2) and linear (η_1) Stark coefficients for the tensor components of some shells around the donor obtained from equation (2). The values are in units of 10^{-3} m^2/MV^2 for η_2 and 10^{-3} m/MV for η_1.

			β		B_{xx}		B_{yy}		B_{zz}		B_{xy}		B_{xz}		B_{yz}	
Class	Shell	Set	η_2	η_1	η_2	η_1	η_2	η_1	η_2	η_1	η_2	η_1	η_2	η_1	η_2	η_1
<0 0 1>	1	(0 0 4)	-3.8	1.7	-3.3	1.6	-4.6	1.9	-3.9	1.8	-3.9	1.8	-0.008	0.6	-0.01	1.4
		(0 4 0)	-3.5	-6.4	-3.3	4.5	-3.8	4.5	-3.8	4.5	-	-	-3.8	4.0	-	-
		(0 $\bar{4}$ 0)	-3.6	9.8	-3.7	-1.0	-3.7	-1.0	-3.7	-1.0	-	-	-	-	-	-
	2	(0 0 8)	-4.1	1.8	-2.8	1.5	-5.1	2.1	-3.9	1.8	-4.5	1.9	-0.004	0.5	-0.006	1.6
		(0 8 0)	-2.2	18.7	-3.7	5.8	-3.8	5.8	-3.7	5.8	-	-	-2.9	-0.27	-	-
		(0 $\bar{8}$ 0)	-2.2	21.5	-3.7	-2.4	-3.7	-2.4	-3.7	-2.4	-6.0	1.6	-2.8	5.5	-	-
<1 1 0>	1	(0 2 2)	-3.8	-1.5	-3.6	2.8	-2.9	7.4	-4.3	-1.8	-3.8	-0.1	-4.0	3.1	-3.9	2.2
		(0 $\bar{2}$ 2)	-3.9	5.0	-3.6	0.6	-2.7	-4.4	-4.4	5.6	-3.8	3.6	-4.0	0.5	-3.9	1.3
		(2 0 2)	-3.6	2.2	-4.4	2.0	-4.4	2.0	-4.4	2.0	-3.8	4.7	-3.9	2.6	-3.8	4.7
	2	(0 4 4)	-3.5	-5.7	-3.5	4.0	-3.4	17.7	-3.6	-9.7	-3.1	-4.9	-4.3	5.0	-3.9	2.9
		(0 $\bar{4}$ 4)	-3.6	9.1	-3.4	0.7	-3.0	14.5	-3.8	13.1	-3.1	8.0	-4.4	1.3	-3.9	0.6
		(4 0 4)	-3.9	3.8	-4.7	3.2	-4.7	3.2	-4.7	3.2	-4.4	26.4	-3.7	3.7	-4.4	26.4
<1 1 1>	1	($\bar{1}$ $\bar{1}$ $\bar{1}$)	-3.8	2.8	-0.1	0.4	0.3	-0.8	-0.1	0.4	-3.9	1.2	-3.8	1.3	-3.9	1.2
		(1 1 $\bar{1}$)	-3.8	0.7	-0.1	-0.3	0.3	0.6	-0.1	-0.3	-3.9	2.4	-3.8	2.2	-3.9	2.4
	2	(3 3 3)	-3.6	-5.6	-0.04	-0.7	0.09	1.5	-0.04	-0.7	-4.2	7.4	-3.1	-3.0	-3.9	7.4
		(3 $\bar{3}$ 3)	-3.7	9.1	-0.06	0.8	0.1	-1.5	-0.06	0.8	-4.2	-3.7	-2.0	6.1	-3.9	-3.7

fine maps of donor wave functions as a means of experimentally characterizing field induced distortions and symmetry changes of the real space wave functions. The nuclear spin of a ^{29}Si atom can essentially act as a probe of the donor wave function, providing a site by site map of the hyperfine interaction to electron localization. Such maps can help us investigate the unknown electronic wave functions in novel Si nanostructures for a host of quantum nanoelectronic applications, and fine tune various modeling techniques at the atomic scale. The predictions of the Stark shift of the hyperfine tensors for six different shells near a P donor indicate that experimental detection of wave function engineering is feasible for lattice sites in the immediate vicinity of the donor, thus providing a probe of the wave function at sub-Bohr radius resolution.

This work was supported by the Australian Research Council, the Australian Government, and the US National Security Agency (NSA), and the Army Research Office (ARO) under contract number W911NF-04-1-0290. Part of the development of NEMO-3D was initially performed at JPL, Caltech under a contract with NASA. NCN/nanohub.org computational resources were used.

Electronic address: park43@purdue.edu

[1] G. P. Lansbergen *et al.*, Nature Physics **4**, 656 (2008).
[2] H. Sellier *et al.*, Phys Rev. Lett. **97**, 206805 (2006).
[3] I. Zutic *et al.*, Rev. Mod. Phys., **76**, 323 (2004).
[4] B. E. Kane, Nature, **393**, 133 (1998).
[5] R. Vrijen *et al.*, Phys. Rev. A **62**, 012306 (2000).
[6] L. Hollenberg *et al.*, Phys. Rev. B **69**, 113301 (2004).
[7] L. Hollenberg *et al.*, Phys. Rev. B **74**, 045311 (2006).
[8] R. de Sousa *et al.*, Phys. Rev. A **70**, 052304 (2004).
[9] M. J. Calderon *et al.*, Phys. Rev. Lett. **96**, 096802 (2006).
[10] D. Loss and D. P. Vincenzo, Phys. Rev. A **57**, 120 (1998).
[11] Srijit Goswami *et al.*, Nature Physics **3**, 41 (2007).
[12] S. R. Schofield *et al.*, Phys. Rev. Lett. **91**, 136104 (2003).
[13] D.N. Jamieson *et al.*, Appl. Phys. Lett. **86**, 202101 (2005).
[14] S. E. S. Andresen *et al.*, Nano Lett. **7**, 2000 (2007).
[15] F. J. Ruess *et al.*, Phys. Rev. B **75**, 123013 (2007).
[16] F. J. Ruess *et al.*, Phys. Rev. B **76**, 085403 (2007).
[17] E. B. Hale and R. L. Mieher, Phys. Rev. **184**, 739 (1969).
[18] G. Feher, Phys. Rev. **114**, 1219 (1959).
[19] E. B. Hale and R. L. Mieher, Phys. Rev. B **3**, 1955 (1971).
[20] J. L. Ivey and R. L. Mieher, Phys. Rev. Lett. **29**, 176-178 (1972); J. L. Ivey and R. L. Mieher, Phys. Rev. B **11**, 849 (1975).
[21] H. Overhof and U. Gerstmann *et al.*, Phys. Rev. Lett. **92**, 087602 (2004).
[22] E. B. Hale and T. G. Castner, Jr., Phys. Rev. B **1**, 4763-4783 (1970).
[23] W. M. Witzel *et al.*, Phys. Rev. B **76**, 035212 (2007).
[24] A. Debernardi *et al.*, Phys. Rev. B **74**, 035202 (2006).
[25] T. B. Boykin *et al.*, Phys. Rev. B **69**, 115201 (2004).
[26] S. Ahmed *et al.*, Encyclopedia of Complexity of Systems (2008) (in press).
[27] G. Klimeck *et al.*, Comput. Model. Eng. Sci. **3**, 601, (2002).
[28] G. Klimeck *et al.*, IEEE Trans. Electron Dev. **54**, 2079, (2007).
[29] R. Rahman *et al.*, Phys. Rev. Lett. **99**, 036403 (2007).
[30] F. R. Bradbury *et al.*, Phys. Rev. Lett. **97**, 176404 (2006).
[31] C. J. Wellard and L. C. L. Hollenberg, Phys. Rev. B **72**, 085202 (2005).

[32] A. S. Martins *et al.*, Phys. Rev. B **69**, 085320 (2004).
[33] G. D. J. Smit *et al.*, Phys. Rev. B **68**, 193302 (2003).